Anti-Kondo effect in Rh-Fe: de Haas–van Alphen observations of scattering anisotropy and exchange energy

L. S. Cheng* and R. J. Higgins
Physics Department, University of Oregon, Eugene, Oregon 97403

J. E. Graebner and J. J. Rubin
Bell Laboratories, Murray Hill, New Jersey 07974

(Received 27 April 1978)

Wave-shape analysis of the de Haas–van Alphen (dHvA) signal on two hole orbits labeled $\alpha(111)$ and $\beta(100)$ in Rh–500-ppm Fe and Rh–700-ppm Fe at $T = 1.2\,^{\circ}\mathrm{K}$ yields values of the exchange field which display no significant field dependence, and a magnitude equivalent to a g-factor shift of -10% (antiferromagnetic) from pure rhodium over the experimental magnetic-field range. No significant ($<2\%$) spin-dependent scattering anisotropy was observed on these orbits. The scattering temperatures measured from the amplitude of first-harmonic dHvA oscillations on $\alpha(111)$, $\beta(100)$, and $\delta(111)$ orbits display very different temperature dependences, with the most d-like orbit [$\delta(111)$] showing the largest temperature-dependent scattering rate and the least d-like orbit [$\alpha(111)$] showing a negligibly small temperature dependence. This proves that the anomalous temperature dependence of the RhFe electrical resistivity is connected with the d-wave nature of the host. We observe that the slope of the resistivity is a factor of 4 smaller than that of the Dingle temperature on d-like $\delta(111)$ orbits over the temperature range between 1.2 and 1.8 °K. An APW calculation of the orbital symmetry character has been performed to facilitate phase-shift analysis of the data. A discrepancy between the experimental results and the phase-shift analysis of the temperature dependence of the scattering rate indicates that the explanation needs something beyond the (Anderson) phase-shift model. Knapp's two-band model and Kondo's hypothesis of simultaneous presence of spin and potential scattering have been ruled out as an explanation of the resistivity anomaly in RhFe, owing to the observed positive temperature dependence of the scattering rate on d-like $\delta(111)$ orbits, and the calculated small potential scattering phase shift, respectively. The localized-spin-fluctuation model (LSF) explains quite well the temperature dependence of the resistivity. However, a calculation of the orbitally averaged scattering rate due to spin fluctuations is necessary to make a direct comparison between the LSF model and our experimental results.

I. INTRODUCTION

The RhFe dilute-alloy system has been a prototype of unusual magnetic-impurity behavior ever since the discovery[1] that its electrical resistivity retained a positive and nearly linear temperature dependence down to 0.02 °K.[2] Because the host is a transition metal, a wider variety of interpretations are possible than in the usual Kondo systems. Explanations proposed include the presence of several bands of differing wave-function symmetry,[3] the simultaneous presence of spin and potential scattering,[4] a temperature-dependent occupation of the spin-down impurity band,[5] and localized-spin-fluctuation (LSF) scattering.[6] However, while several such models describe the gross features of the bulk measurements, they involve very different pictures of the underlying microscopic state.

Landau quantum oscillations of the magnetic susceptibility [the de Haas–van Alphen (dHvA) effect[7]] can be used to measure very specific properties of the impurity-electron interaction. The dHvA effect is produced by the electrons on well-defined orbits on the Fermi surface (FS), whose wave-function symmetry can be calculated. Since the applied field polarizes the spin of the conduction electrons, information about the spin-dependent part of the interaction can be deduced. Recently, analysis of the wave shape[8,9] of dHvA oscillations has been developed which yields the spin-dependent self-energy[10] characterizing the electron-impurity interaction. Thus, the dHvA effect provides a detailed, microscopic model-independent picture of the impurity-host interaction.

This project was undertaken in an attempt to provide, using dHvA techniques, direct *microscopic* information on the scattering, its temperature dependence and k-space anisotropy, and on the exchange energy of the Fe impurity in Rh. Preliminary results have

been reported earlier.[11] A more detailed description is given elsewhere.[12] The following goals have been achieved in this experiment. First, a comparison of scattering rates on Fermi-surface sheets of differing symmetry explains the nature of the coupling and yields the impurity phase shifts. Second, the temperature dependence of the total scattering rate on several FS sheets is observed and compared with the resistivity. Third, measurements of g-factor shifts and of the spin dependence of the scattering yields the microscopic values of the exchange energy and the full spin-dependent self-energy.

A. dHvA effect in the presence of magnetic impurities

The dHvA effect in nonmagnetic metals containing magnetic impurities can be taken into account phenomenologically by a modification[10,13] of the Lifshitz-Kosevich formula

$$M_{\rm osc}=-\sum_{r=1}^{\infty}\tfrac{1}{2}C_r D^r[E^{-2r}+E^{2r}+2\cos(2\pi rS)\,]^{1/2} \times\sin[2\pi r(F'/H-\lambda)\pm\tfrac{1}{4}\pi+\Delta\theta_r]\ , \quad (1a)$$

where

$$C_r=\nu TF/\left[\left(rH\frac{d^2A_k}{dk_H^2}\right)^{1/2}\right]2\sinh\left(\frac{r\lambda_0 m^*T}{H}\right)\ ,$$

$$D=\exp(-\lambda_0 m^*\bar{T}_D/H)\ , \quad (1b)$$

$$E=\exp(-\lambda_0 m^*\Delta\bar{T}_D/H)\ .$$

Here we have $F'=F-\Delta F$ (ΔF is the shift in dHvA frequency due to alloying),

$$\Delta\theta_r=\tan^{-1}\left[\tan(\pi rS')\left(\frac{1-E^{2r}}{1+E^{2r}}\right)\right]\ , \quad (1c)$$

$$\Delta F/H=(\Sigma_\uparrow'+\Sigma_\downarrow')/2\hbar\omega_c\ ,$$

and

$$\bar{T}_D=-(\Sigma_\uparrow''+\Sigma_\downarrow'')/2\pi k_B$$

is the mean Dingle temperature for up-spin and down-spin electrons, and

$$\pi k_B(T_{D\uparrow}-T_{D\downarrow})=\pi k_B\Delta T_D=(\Sigma_\uparrow''-\Sigma_\downarrow'')/2 \quad (1d)$$

is a measure of the spin-dependent scattering, and

$$S'=\left(\frac{\mu_B H}{\hbar\omega_c}\right)\left(g_c+\frac{\Sigma_\uparrow'-\Sigma_\downarrow'}{\mu_B H}\right)=\tfrac{1}{2}m^*\left(g_c-\frac{H_{\rm ex}}{H}\right) \quad (1e)$$

is a measure of the spin splitting of energy levels, $H_{\rm ex}$ is defined as the exchange field where

$$\Sigma_\sigma=\Sigma_\sigma'-i\,\mathrm{sgn}\,\Sigma_\sigma'' \quad (1f)$$

is the conduction-electron self-energy, and σ represents the spin of the electron. The absolute amplitude is set by

$$\nu=[4k_B/(2\pi)^{1/2}]\left(\frac{e}{\hbar c}\right)^{3/2} =1.304\times10^{-5}\ \mathrm{Oe}^{1/2}/\mathrm{K}\ , \quad (1g)$$

$$\lambda=2\pi^2k_Bc/he=146.9\ \mathrm{kG/K}\ .$$

Thus, a measurement of $\bar{T}_D$ ΔT_D, ΔF, and $H_{\rm ex}$ can yield information on both the real and the imaginary parts of the self-energy for up- and down-spins. Experimentally, the information is determined by precise measurement of amplitudes and phases θ_r of various harmonics, where θ_r is defined

$$\theta_r=2\pi r(F/H-r)\pm\tfrac{1}{4}\pi+\Delta\theta_r\ , \quad (2)$$

using methods of analysis described earlier.[9,13] With the detection of the first three harmonics and the phase difference $2\theta_1-\theta_2$, $3\theta_1-\theta_3$ [see Fig. 1 and Eq. (1)], it is possible to calculate directly the spin-dependent scattering (SDS) and exchange energy (EE) at a single value of magnetic field and temperature.

B. Theoretical models for the effect of magnetic-impurity scattering on the dHvA effect

a. Based on the s-d exchange Hamiltonian, the self-energy of the impurity–conduction-electron

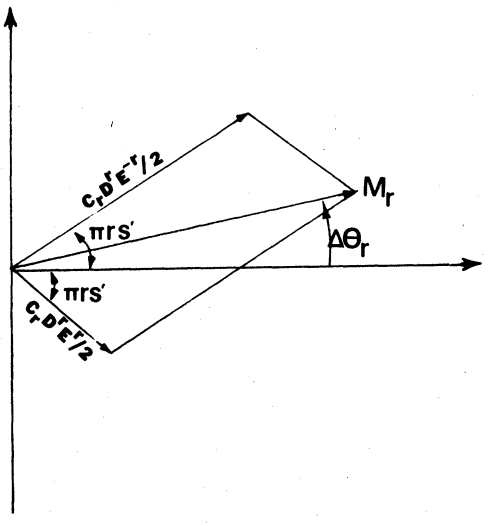

FIG. 1. Phasor diagram of the rth dHvA harmonic amplitude (M_r) defined in Eq. (1) in the presence of spin-dependent scattering anisotropy (SDS). $\Delta\theta_r$ is the SDS-induced phase shift. $\pi rS'$ is the spin-splitting angle.

interaction is

$$\Sigma_\sigma(i\omega)=\frac{-c}{\pi\rho}\sin\delta_\nu\exp[i\delta_\nu\,\mathrm{sgn}(\omega)] +\exp[2i\delta_\nu\,\mathrm{sgn}(\omega)]t_{\bar{J}\sigma}(i\omega) \ , \tag{3}$$

where c is the concentration of impurities, ρ is the density of states, δ_ν is the phase shift due to potential scattering, and $t_{\bar{J}\sigma}$ is the t matrix of the scattering due to the s-d exchange interaction, with the replacement

$$\bar{J}=J\cos^2\delta_\nu \ .$$

Thus, Harris *et al.*[14] evaluate the self-energy based on the assumption that the exchange interaction arises primarily from a resonant interaction between the d-wave part of the conduction-electron wave function and the localized d states on the impurity,[15,16] and obtain

$$\pi K_B\Delta T_D=-c\sum_M 2\alpha\beta(1+r)\,\mathrm{Re}(T_\uparrow^J-T_\downarrow^J) \ , \tag{3a}$$

$$g\mu_B H_{\mathrm{ex}}=c\sum_M \alpha[(1+r)^2-\beta^2]\,\mathrm{Re}(T_\uparrow^J-T_\downarrow^J) \ , \tag{3b}$$

$$\pi k_B\bar{T}_D=-c\sum_M\{\alpha\epsilon+\alpha[(1+r)^2-\beta^2] \times\tfrac{1}{2}\,\mathrm{Im}(T_\uparrow^J+T_\downarrow^J)\} \ . \tag{3c}$$

The parameters α, β, r, and ϵ are defined as follows:

$$\begin{aligned}&\alpha=\langle|b_{LM}(K)|\rangle_{\mathrm{orbit}} \ ,\\ &\beta=\pi\rho\langle|b_{LM}(K)|^2\rangle_{\mathrm{FS}}\,\mathrm{Re}A_L t_L \ ,\\ &r=\pi\rho\langle|b_{LM}(K)|^2\rangle_{\mathrm{FS}}\,\mathrm{Im}A_L t_L \ ,\\ &\epsilon=\mathrm{Im}A_L t_L \ ,\end{aligned} \tag{4a}$$

and

$$t_L=-(E_F)^{1/2}\sin\Delta\eta_L \ . \tag{4b}$$

Here A_L are the backscattering coefficients; $|b_{LM}(K)|^2$ represents the amount of s-, p-, and d-like character of the Bloch state, and the notation $\langle|b_{LM}(K)|^2\rangle_{\mathrm{orbit}}$ and $\langle|b_{LM}(K)|^2\rangle_{\mathrm{FS}}$ stand for the average around the orbit and the average over the Fermi surface, respectively. $\Delta\eta_L$ represents the difference between the phase shift of host and the impurities at the Fermi energy; $\mathrm{Re}A_L$ and $\mathrm{Im}A_L$ are the real and imaginary parts of backscattering coefficients; the $\sum_M$ denotes the summation of the d-like representations Γ_{12} and Γ_{25} of the cubic group, and T_σ is the temperature-dependent t matrix containing the information about the exchange scattering.

Thus, we can rewrite[17] Eq. (4) as follows:

$$\pi k_B\bar{T}_D=\frac{\hbar^2 c}{2\pi m^*}\sum_L \mathrm{Im}S_L\left(\frac{\partial A}{\partial\eta_L}\right)_{E_F} -c\alpha[(1+r)^2-\beta^2]\tfrac{1}{2}\,\mathrm{Im}(T_\uparrow^J+T_\downarrow^J) \ , \tag{5a}$$

where $\mathrm{Im}S_L$ are the scattering parameters defined as

$$\mathrm{Im}S_L=A_L\sin\Delta\eta_L\,e^{i\Delta\eta_L} \ , \tag{5b}$$

$(\partial A/\partial\eta_L)_{E_F}$ are the derivatives of the area of the orbit with respect to the phase shifts, and are the means by which the symmetry character of the host determines the relative orbital-scattering anisotropy. As indicated in Eq. (5), the scattering rate has a contribution from both potential scattering and temperature-dependent exchange scattering.

b. Based on the Anderson model, Shiba[10] related the self-energy to the d-wave phase shift, under the assumptions that the inelastic scattering can be ignored and only the d-wave scattering phase shift is important.

$$\Sigma_\sigma=-a_{\mathrm{orb}}\frac{5c}{\pi\rho}\sin\eta_\delta\,e^{i\eta_\sigma} \ , \tag{6a}$$

where

$$a_{\mathrm{orb}}=\frac{\sum_{m=-2}^{2}\langle|V_{km}|^2\rangle_{\mathrm{orb}}}{\sum_{m=-2}^{2}\langle|V_{km}|^2\rangle_{\mathrm{FS}}} \tag{6b}$$

and V_{km} is the transition rate describing the s-d mixing character. Through the Friedel sum rule, we can obtain

$$\pi k_B\bar{T}_D=a_{\mathrm{orb}}\frac{5c}{\pi\rho}(\tfrac{1}{2}\sin^2\eta_\uparrow+\tfrac{1}{2}\sin^2\eta_\downarrow) \ , \tag{7a}$$

where, following Nagasawa,[12] we have

$$\begin{aligned}&\eta_\uparrow=\tfrac{1}{5}\pi[N_\uparrow(T)-\eta_0] \ ,\\ &\eta_\downarrow=\tfrac{1}{5}\pi[N_\downarrow(T)-\eta_0] \ ,\end{aligned} \tag{7b}$$

where N is the d-electron number of the impurity atom for each spin component, η_0 is that of the host-metal atom, and

$$\begin{aligned}&N_\uparrow(T)=N(0)+N'(T) \ ,\\ &N_\downarrow(T)=N(0)-N'(T) \ .\end{aligned} \tag{7c}$$

The difference $N_\uparrow(T)-N_\downarrow(T)$ contributes to the magnetic susceptibility, and appears to vanish at 0 °K (nonmagnetic ground state).[12] We can rewrite Eq.(7) as:

$$\pi k_B\bar{T}_D=a_{\mathrm{orb}}\left(\frac{5c}{\pi\rho}\right)\{Q\} \ ,$$

$$\{Q\}=\sin^2\{\tfrac{1}{5}\pi[N(0)-\eta_0]\} +\cos\{\tfrac{2}{5}\pi[N(0)-\eta_0]\}\sin^2[\tfrac{1}{5}\pi N'(T)] \ . \tag{8}$$

Thus a simple phase-shift calculation is presented which relates the temperature dependence of the

non-spin-flip scattering to the temperature dependence of the impurity magnetic moment through the quantity $N'(T)$.

c. In analogy to localized spin fluctuations (LSF) *in resistivity,* the Dingle temperature may be expressed as the sum of a potential scattering term plus LSF scattering rate $(1/\tau)_{\mathrm{LSF}}$ as follows:

$$\pi k_B \bar{T}_D = \frac{\hbar^2 c}{2\pi m^*} \sum_L \mathrm{Im} S_L \left(\frac{\partial A}{\partial \eta_L} \right)_{E_F} + (\hbar/\tau_{\mathrm{LSF}}) \ , \qquad (9)$$

where $(1/\tau)_{\mathrm{LSF}} = 0$ when $T = 0\,^{\circ}\mathrm{K}$, varies initially as T^2 and then as T, by analogy with the resistivity.[6]

In this approach, the temperature dependence of the scattering rate is due to scattering of conduction electrons from time-dependent fluctuations of the magnetization at the site of a magnetic transition-metal impurity (i.e., LSF). Such a model explained the resistivity behavior in RhFe, IrFe, and similar alloys (Coles alloys) quite well,[6] and showed that the resistance anomaly in Coles alloys is of the same nature as the Kondo anomaly. The impurity magnetic moment may be thought to exist with a relatively fixed magnitude, but with fluctuations in lifetime. The fluctuation "temperature" (T_{sf}) varies widely, depending on the host. The difference between Coles and Kondo alloys lies in the coupling between the conduction electrons and the LSF. Kondo alloys with host and impurity of *different* electronic structure are best described by the Anderson model, which includes an extra d orbital, characteristic of the impurity, in addition to the host states $|k\rangle$. Thus, the conduction electrons in Kondo alloys must first tunnel into an extra d orbital where the LSF take place.[18] Coles alloys with host and impurity of the *same* electronic structure can be described more naturally by the Wolff model,[19] which implies a single-band description of the alloy.

All of these three models are considered later in interpreting the RhFe data.

II. PHASE-SHIFT ANALYSIS OF THE FERMI SURFACE OF RHODIUM

The k-space anisotropy of each partial wave contribution to both potential and exchange (s-d and d-d) scattering rates depends on the anisotropy of the host-metal wave functions at the Fermi energy.[14,17] The determination of wave-function symmetry is therefore important in understanding the anisotropy in scattering rate (and its temperature dependence) on different extremal orbits of the Fermi surface. The symmetry information required for a partial wave fit to Eq. (5) is $(\partial A/\partial \eta_l)_{E_F}$ (i.e., the sensitivity of the orbital area to partial wave shifts). Such information has been calculated in noble metals[20,21] and a few transition metals[22] (Molybdenum and Tungsten) by parametrization of Fermi surfaces using KKR or APW band-structure calculations, adjusting the s, p, and d phase shifts to obtain agreement with the experimental Fermi-surface dimensions. Reliable results were obtainable because the Fermi surface of these metals is well known. However, an empirical phase-shift analysis is complicated for a transition metal such as Rhodium by the fact that the large Γ-centered electron sheet of the Fermi surface (see Figs. 2 and 3) is not well known enough to pin down the phase shifts uniquely. Although one could certainly *parametrize* using what is known about the smaller sheets, the resulting phase shifts could yield very different pictures of the large sheets—a nonuniqueness problem. We were therefore led to develop a combined scheme, which used the augmented-plane-wave (APW) method to arrive at a *first-principles* band structure, trimmed up by an adjustment of the Fermi energy to fit what is known of the Fermi surface. The method leads to a consistent fit to the experimental FS data. It is reassuring to note that the symmetry of various orbits in Rhodium turned out to be insensitive to this trimming up procedure. This is the first time that the first-principles APW method has been used to extract symmetry information for a scattering calculation, rather than using a parametrization.

A. Augmented-plane-wave calculation of Fermi surface and orbital symmetry

The muffin-tin potential used in the present calculations was derived from atomic Dirac-Hartree-Fock-

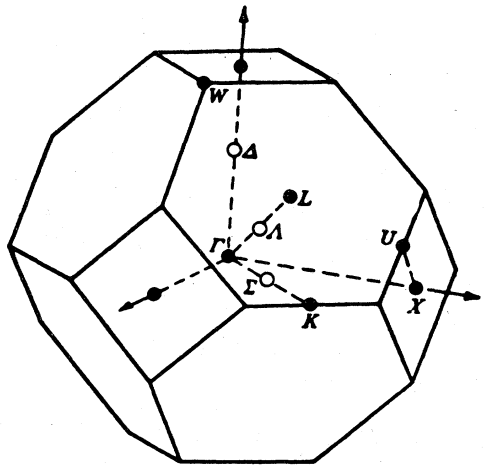

FIG. 2. Brillouin Zone of the face-centered-cubic lattice showing the conventional labeling of high-symmetry points and lines.

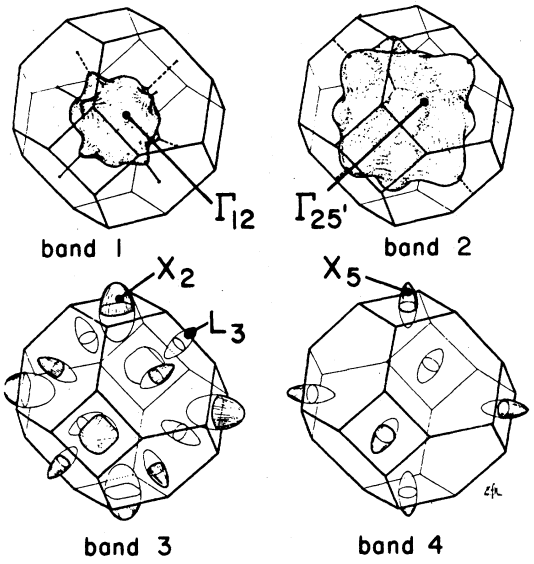

FIG. 3. Schematic diagram showing the various sheets of the Fermi surface, determined by Coleridge (Ref. 27), with symmetry labeling from APW (Refs. 26,28). Band 1: A closed electron sheet depressed along the ΓK directions (Γ_{12} or δ orbits). Band 2: A closed electron sheet pulled out along the ΓK directions (Γ_{25}'). Band 3: A set of hole pockets around the points X (X_2 or γ orbits) and a smaller set around L (L_3 holes or α orbits). Band 4: A set of hole pockets around X (X_5 or β orbits).

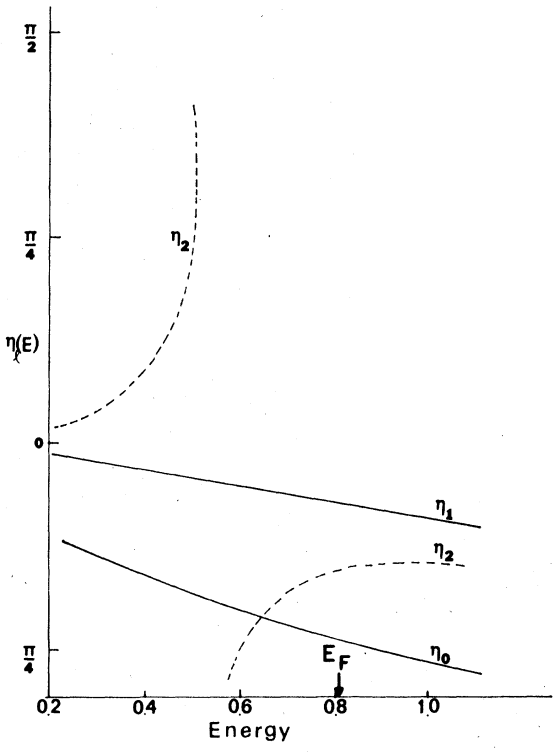

FIG. 4. Energy-dependent scattering phase shifts $\eta_l(E)$ which characterize the scattering of electrons due to a "muffin-tin" potential in rhodium calculated as a function of energy for pure rhodium.

Slater charge densities,[23] using full Slater exchange and assuming a $4d^8 5s^1$ charge configuration. Energy eigenvalues and wave functions were calculated using the APW method, following the calculational procedures outlined by Loucks.[24] The partial wave-scattering phase shifts $\eta_L(E)$, which characterize the scattering of electrons due to the muffin-tin potential, were calculated from

$$\tan\eta_L(E) = \frac{R_L'(S_\nu,E)J_L(Kr) - R_L(S_\nu,E)J_L'(Kr)}{R_L'(S_\nu,E)Y_L(Kr) - R_L(S_\nu,E)Y_L'(Kr)}, \tag{13}$$

where $E = K^2$, Y_L is the spherical Neumann function, and $R_L'(S_\nu)/R_L(S_\nu)$ is the logarithmic derivative of the solution of the radial Schrödinger equation for angular momentum L evaluated at the "muffin-tin" radius S_ν.

The resulting APW phase shifts are shown plotted as a function of energy in Fig. 4. Note that the d electrons go through a scattering resonance at $E = 0.6$ Ry. The energy bands were calculated along high-symmetry directions.[12] The eigenvalues agree with Andersen's values[25] to within 0.01 Ry.

Extremal areas and their derivatives with respect to η_L were calculated by extending the APW secular equation away from symmetry directions into general directions in k space (see Ref. 12 for details). The values of η_L were those determined from the band calculation along symmetry lines. Procedures for orbit tracing and area integration are described elsewhere.[26] E_F was adjusted to optimize the agreement with experimental dHvA extremal areas. Extremal areas generated by this procedure are given in Table I. The close correspondence between these results and the results (also shown in Table I) of a previous band calculation[26] and with the experimental data is a check on the following extension of the band calculation to generate symmetry information.

The derivatives $\partial A/\partial\eta_L$ were calculated using a finite-difference technique, varying η_L by a small amount (−0.002 Rad) at fixed E_F, and repeating the above orbit-tracing calculation.

The results in Table II (at $E_F = 0.81$ Ry) show that two large Γ-centered electron sheets and γ orbits (holes at X) are predominately d-like, and the α orbits (holes at L) and β orbits (holes at X) are of mixed p-d symmetry. Since the Fermi energy is the only parameter (adjusted to fit the Fermi surface), it is of interest to verify that the symmetry character of these orbits is not strongly sensitive to E_F. Table III

TABLE I. Comparison of the Fermi-surface extremal areas of Rhodium in the present work ($E_F = 0.81$ Ry) with Andersen's calculation (Ref. 26) and the dHvA experimental measurements (Ref. 27 and this experiment).

FS sheet	Magnetic-field direction	Extremal Areas (a.u.) Andersen	Present work	Experiment
	[111]	0.539	0.547	0.547
Electron	[100]	0.603	0.610	0.622
Γ_{12}	[110]	0.699	0.720	0.690
Electron	[111]	1.505	1.506	· · ·
$\Gamma_{25'}$	[100]	1.532	1.563	· · ·
Hole (β)	[100]	0.0457	0.0482	0.0417
X_5	[010]	0.0690	0.0712	0.0658
Hole (γ)	[010]	0.1618	0.1651	· · ·
X_2				
Hole (α)	[111]	0.0072	0.0062	0.0062
L_3	[112]	· · ·	0.0065	0.0065
	[110]	· · ·	0.0072	0.0072

TABLE II. The symmetry character, i.e., the sensitivity of various orbits to partial wave phase shifts on the extremal orbits of Rhodium for $E_F = 0.81$ Ry.

	Direction	$(\partial A/\partial\eta_0)^a$	$\left(\frac{1}{m^*}\frac{\partial A}{\partial\eta_0}\right)$	$\frac{\partial A}{\partial\eta_1}$	$\left(\frac{1}{m^*}\frac{\partial A}{\partial\eta_1}\right)$	$\frac{\partial A}{\partial\eta_2}$	$\left(\frac{1}{m^*}\frac{\partial A}{\partial\eta_2}\right)$
Electron	[111]	0.06	0.03	0.10	0.05	2.47	1.24
Γ_{12}	[100]	0.08	0.03	0.14	0.05	3.51	1.37
	[110]	0.06	0.02	0.13	0.04	4.40	1.42
Electron	[111]	0.03	· · ·	0.17	· · ·	7.46	· · ·
$\Gamma_{25'}$	[100]	0.03	· · ·	0.20	· · ·	6.83	· · ·
Hole (β)	[100]	0.00	0.00	−0.12	−0.26	−0.44	−0.96
X_5	[010]	0.00	0.00	−0.09	−0.15	−0.70	−1.13
Hole (γ)	[010]	0.02	· · ·	−0.10	· · ·	−2.23	· · ·
X_2							
Hole (α)	[111]	0.00	0.00	−0.09	−0.66	−0.10	−0.73
L_3	[112]	0.00	· · ·	−0.10	· · ·	−0.11	· · ·
	[110]	0.00	· · ·	−0.11	· · ·	−0.11	· · ·

[a]Units: A is measured as a fraction of the free-electron sphere cross section for Rh, and η is in radians.

TABLE III. The symmetry character, i.e., the sensitivity of various orbits to partial wave phase shifts on the extremal orbits of Rhodium, calculated at several values of E_F. The units are as in Table II.

	E_F	Magnetic-field direction	Extremal area	$\frac{\partial A}{\partial \eta_0}$	$\frac{\partial A}{\partial \eta_1}$	$\frac{\partial A}{\partial \eta_2}$
Electron	0.78	[111]	0.385	0.03	0.06	2.62
Γ_{12}	0.81	[111]	0.547	0.06	0.10	2.47
	0.84	[111]	0.679	0.12	0.25	2.12
Hole (β)	0.70	[100]	0.218	0.00	−0.41	−0.50
X_5	0.78	[100]	0.0825	0.00	−0.20	−0.48
	0.81	[100]	0.0482	0.00	−0.12	−0.44
Hole (α)	0.70	[111]	0.108	0.00	−0.55	−0.34
L_3	0.81	[111]	0.0062	0.00	−0.09	−0.10

shows that the extremal areas of the smaller orbits are strongly sensitive to a shift in E_F. Since the areas are well known (to ~1%), E_F is located rather closely (~0.01 Ry). It follows from Table III that 0.01-Ry uncertainty in E_F limits to at most 3% the uncertainty in symmetry character (for s, p, and d waves) for these orbits.

A check on these symmetry calculations is provided by noting in Table III that as E_F increases, the symmetry of the extremal Fermi surface associated with the Γ_{12} electron will be more s- and p-like and less d-like, but α and β orbits will show more d-like behavior. The result is consistent with the energy-band calculations.[16,17] As the Fermi energy is increased, the Γ_{12} electron moves away from crossing the d resonance, becoming more free electronlike, while the smaller hole sheets approach symmetry points where group theory indicates the symmetry is purely d-like (L_3,X_5).

Previous inferences[28] about the symmetry character of the conduction electrons on the FS of Rh (based on the shape of the energy bands, variation in magnitude of the Fermi velocity on the different FS sheets, and the low density of states on the Γ_1 electron sheet) suggested that the hole orbits were primarily d-like and the Γ_{12} electrons were the most s-p-like sheet, which disagrees with the above calculation. However, those earlier assignments of symmetry character were indirect inferences of qualitative value only, and the quantitative results of our partial wave analysis are expected to be more reliable.

III. EXPERIMENTAL CONSIDERATIONS

The high magnetic field and low temperature needed for most of the dHvA measurements were obtained using a 55-KG superconducting solenoid and a ^{4}He cryostat with temperature range from 4.2 to 1.2 °K. Due to the complexity of Fermi surface in transition metals and the large effective masses on certain orbits, the experiments are quite complicated compared to similar studies on noble-metal hosts.[9,16] The small hole pockets around L (α orbits) and X (β orbits) with small effective masses are good candidates for dHvA measurements, but because of the complex beat patterns due to the families of symmetrically equivalent ellipsoidal pockets, reliable dHvA amplitude and relative phase measurements at arbitrary direction of H proved unfeasible. For the hole orbits, the most reliable data were obtained for $\vec{H} \parallel [111]$ on the L holes and for $\vec{H} \parallel [111]$ on the X_5 holes. The measurements on two large Γ-centered electron sheets, $\Gamma_{25'}$ ($m^* \simeq 4m_0$) and Γ_{12} ($m^* \simeq 2m_0$), were limited by our accessible magnetic and temperature range. The most reliable data on Γ_{12} were obtained for $\vec{H} \parallel [111]$ and in fields extended up to 80 kG. $\Gamma_{25'}$ proved unfeasible with our apparatus.

A. Sample preparation

The Rhodium and RhFe single crystals used in this work were grown at Bell Laboratories using the electron-beam floating-zone method. Alloy crystals were grown by splitting a pure Rh crystal and inserting an Fe wire, followed by repeated zone leveling. Rectangular dHvA samples with the long axis at the [111] or [100] direction were cut by spark erosion and the sample was etched elecrolytically (sample size: $1 \times 1 \times 2$ mm ^{3}) to remove the surface damage. The sample was mounted in a large-angle rotator and could be oriented anywhere in the (110) plane to reach the principal symmetry directions during the

same experiment, avoiding amplitude errors due to thermal cycling. Representative samples from the single crystals were analyzed using atomic-absorption spectroscopy. The Fe concentrations were found to be 500, 700, 1100, and 2100 ppm in the samples used in this work, and showed insignificant gradients in composition over the length of a sample.

B. Field-modulation technique

A sinusoidal modulation field $h = h_m \cos\omega t$ generated by a Helmholtz pair is superimposed on the steady field H_0. The signal V induced in the pick-up coil is rich in harmonics of frequency $n\omega$ due to the nonlinear dependence of the magnetization of the sample. The signal V can be expressed as[29,30]

$$V \alpha \sum_r A_r \sum_{n=1}^{\infty} n\omega J_n(\lambda_r) \sin(n\omega t + \tfrac{1}{2}n\pi) \times \sin[2\pi r(F/H - \gamma) \pm \tfrac{1}{4}\pi + \tfrac{1}{2}n\pi] \ , \quad (14)$$

where $\lambda_r = 2\pi r F h_m / H^2$.

The pick-up coil voltage contains all harmonics of the modulation frequency with the amplitude modified by Bessel functions. Since the modulation amplitude was adjusted to be proportional to the square of the magnetic-field strength, the Bessel-function argument λ_r does not vary during the field sweep, simplifying the analysis.

A particular value of λ_r could be selected to enhance or eliminate a particular dHvA frequency. Because of the complex frequency spectrum due to the multiple sheets of FS, the detection harmonic and the value of λ_r had to be carefully chosen for each case. For example, the 4th harmonic and $\lambda = 5.32$ (the first peak of J_4) were selected for the measurement of the Dingle temperatures for X_5 (100). The oscillations of L (100) are greatly attenuated in spite of its smaller effective mass [$m^*(L) \simeq m^*(X_5)/3$], because the two differ in dHvA frequency by a factor of 10, and the L-hole signal finds itself on the leading edge of $J_4(\lambda)$ and significantly reduced in amplitude ($J_4 \propto \lambda^4$, $\lambda << 1$).

C. DHVA amplitude measurement and analysis

A computer-centered automated system was used to control all the experimental parameters (except temperature) and to process and store data.[31] The temperature of the helium bath was controlled by a vacuum-regulator valve (Lake Shore Cryotronics). The pressure drift during the experiment was less than 0.1 Torr. For a more precise temperature readout, a strontium-titanate glass-ceramic cryogenic capacitance sensor (Lake Shore Cryotronics) was mounted on the bottom of the experimental probe, together with a heater used for temperature regulation below 2 K.

Harmonics of the modulation frequency generated by the sample were processed with a software multichannel phase-sensitive detector.[32] In order to get reliable measurements of the amplitude of the fundamental and higher harmonics of the frequency of interest, a successive subtraction of stronger components in the Fourier spectrum was used to reveal weak Fourier components.[33] This experiment required a substantial advance in the methods of precise spectral analysis. Since much of the interest was in analyzing spin-dependent scattering and g shifts, it was necessary to extract not only the fundamental amplitudes but also harmonic amplitudes *and phases* [e.g., the $\Delta\theta_r$ in Eq. 1(c)]. The problem was that harmonics of interest often were near in frequency to an unrelated Fourier component from a member of the same family of ellipsoids. Simulation experiments showed that Fourier decomposition could reliably extract the *amplitude* of a relatively weak shoulder, but the slight shift in the frequency of the hidden peak resulted in a significant error in the *phase*. An example is shown in Fig. 5. A least-squares fit and subtraction of the interfering peak M_1' revealed the harmonic M_2 with computed amplitude within 3% of input but with phase in error by 5 degrees. As a result, measurements were restricted to a limited choice of field directions, selected so that errors of this sort are limited to 2% for the harmonic amplitudes and 2° for the relative phases.

D. Skin-depth effects

The modulation field and the dHvA signal propagating in the sample may be modified in amplitude and phase by induced currents. The signal is then proportional to a complex "modified Bessel function" (MBF) $J'(\lambda')$ so that in-phase and out-of-phase components appear at the pick-up coil.[9] Both components are detected simultaneously by the multichannel phase-sensitive detection program. One potential error is the variation with H of the effective volume of sample, due to magnetoresistance, leading to an error in Dingle temperature determined from amplitudes as a function of H ("slope Dingle temperature"). The skin depth of the sample δ is related to the magnetic field by

$$\delta = c/[2\pi\omega\sigma(H)]^{1/2} \ , \quad (15)$$

where c is the speed of light, ω is the modulation frequency, and $\sigma(H)$ is the conductivity of the sample in the magnetic field H.

In the Dingle-temperature measurements on hole

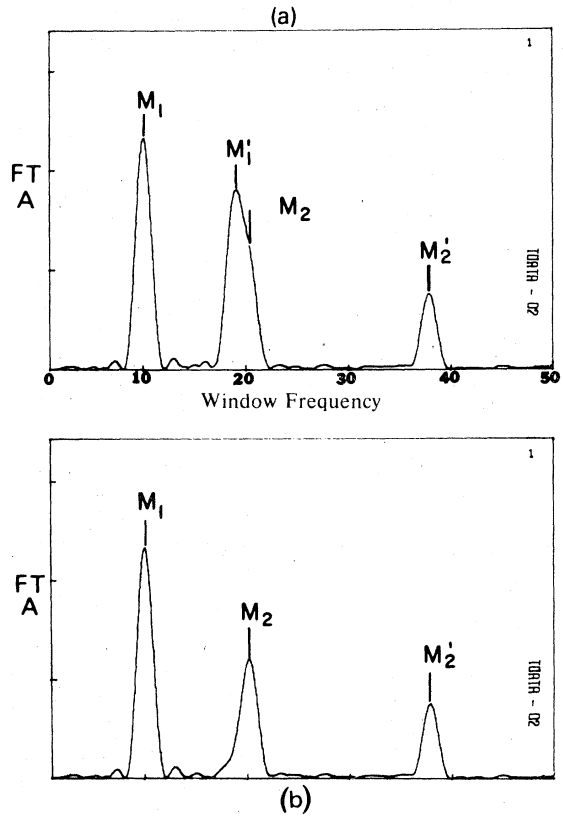

FIG. 5. Computed example of subtracting an interfering but unrelated Fourier component to reveal a harmonic of interest. Shown plotted is the Fourier transform (FT) amplitude (A) as a function of dHvA frequency in cyles per window. (a) is the original computed data, with fundamental M_1 and second-harmonic M_2, together with a second oscillation M_1' (and second-harmonic M_2'), which is separated by less than 1 peak width from M_2. A least-squares fit of peak M_1', and then a subtraction of it from the data results in a transform (b) in which M_2 is now clearly revealed. The amplitude of M_2 is determined to within 2%, but its phase is in error by 5°, due to a slight (1%) shift in its apparent frequency resulting from the subtraction process. The numerical results are

		Frequency (cycles/window)	Amplitude	Phase (deg)
M_1	input	10.200	2.20	35.2
	original FT (a)	10.197	2.22	35.8
	M_1' subtracted (b)	10.191	2.20	36.7
M_2	input	20.400	1.10	67.0
	original FT (a)	Indeterminate	Indeterminate	Indeterminate
	M_1' subtracted FT (b)	20.382	1.12	72.4

orbits in *pure* Rh, the magnetoresistance varies over the field range, so the modulation frequency was kept low enough ($\omega = 17$ Hz) to penetrate the sample completely, avoiding field-dependent skin depth. The skin depth δ estimated in the pure Rh sample [with residual resistance ratio (RRR) ~600 at 20 kG] is ~1 mm, which is about the dimension of the sample. In order to double check the Dingle temperature results, the *harmonic* Dingle temperature was measured from the ratio of first- and second-harmonic amplitudes (the skin-depth effect drops out in the harmonic ratio) and found to be identical to the slope Dingle temperature measurements within the experimental error.

In alloys with 0.05% or more Fe, due to the larger resistance, it was possible to use larger ω (40 hZ),

speeding the data taking. A complete penetration of the sample ($\delta \sim 2$ mm) was verified experimentally by measuring the amplitude as a function of λ at fixed H and demonstrating that it fit an ideal Bessel function.[12]

In the wave-shape analysis measurements, precise amplitude ratios are needed. To correct the observed amplitudes for possible small deviations from the ideal Bessel function, two (three) data blocks were taken at the same field value, using twice (triple) the modulation-field amplitude as the first data block. As shown earlier,[9] the appropriate correction factor for A_2/A_1 or A_3/A_1 is simply the ratio of observed *first-harmonic* amplitudes[9] at double or triple modulation.

IV. RESULT AND DISCUSSION

A. Measurements of effective masses in Rhodium and RhFe

Precise values of effective mass m^* are extremely important in alloy scattering studies. Since the observable is the product m^*T_D, the uncertainty in scattering temperature T_D is related to the uncertainty in m^* by

$$\Delta T_D/T_D = (\Delta m^*/m^*)(1 + T/T_D) \quad . \tag{16}$$

Thus, a 1% error in m* translates to a 5% error in a 1-°K value of T_D measured at a temperature of 4 °K (worst case), and decreases at lower temperatures.

The temperature dependence of the dHvA amplitude $M_1(H)$ at constant H was measured to deduce m^* by plotting $\ln[CM_1(H)/T]$ as a function of T. The plot is a straight line with the slope S related to m^* by

$$m^* = -SH/\lambda \quad .$$

Here, we have made the approximation

$$[\sinh(\lambda m^* T/H)]^{-1} \simeq 2\exp(-\lambda m^* T/H) \quad .$$

This is accurate in this case. The worst case occurs for L holes, where $\lambda m^* T/H > 2.2$ ($T = 1.2$ K and $H = 10$ kG), and the value of $[\sinh(\lambda m^* T/H)]^{-1}$ and $2e^{-\lambda m^* T/H}$ differ only by 1%. Since m^* values measured from 2ω, 4ω, 6ω, and 8ω detection-frequency channels agreed within 1%, no problem of skin depth versus temperature [which might cause a spurious $T_D(T)$ measurement] was observed. The comparison of the effective-mass measurements in this work with Hornfeldt's results (private communication) and theoretical calculation are shown in Table IV. The two measurements agree well for the δ and β orbits.

The assumption was made that the pure Rh m^* values are unchanged in dilute RhFe alloys. The problem is that an alloying shift Δm^* is inseparable

TABLE IV. Comparison of the effective mass (m^*) of Rhodium in present work with the dHvA experimental measurements of Hornfeldt (private communication) and Andersen's theoretical calculation (Ref. 26). The values used in interpreting the temperature dependence of X_D are shown underlined.

	Direction	Theoretical Calculation	Hornfeldt	Present Work
Electron	[110]	2.27	3.1 ± 0.3	· · ·
(δ)	[111]	1.43	<u>1.98 ± 0.05</u>	1.99 ± 0.07
Γ_{12}	[100]	· · ·	2.8 ± 0.1	2.99 ± 0.07
	24°[b] from [100] toward [111] along (110) plane	· · ·	2.56 ± 0.03	2.82 ± 0.05
Hole (β)	[100]	0.35	<u>0.453 ± 0.007</u>	0.46 ± 0.03
X_1	[010]	0.48	0.62 ± 0.02	0.65 ± 0.02
Hole (γ)	[110]	0.99	1.15 ± 0.05[b]	1.431 ± 0.015
X_2		0.91		
Hole (α)	[111]	0.11	0.137 ± 0.003	<u>0.132 ± 0.002</u>
L				

[a]22° from [100] toward [111] along (110) plane in our measurement.

[b]An off-central orbit.

from a temperature-dependent scattering $X(T)$. The assumption is justified by our observation of no alloying shifts in FS *area*, which other experiments have shown are larger than changes in m^*.

B. Magnetic interaction (MI)

Wave-shape analysis depends upon the harmonic content of dHvA oscillations. Since the electrons in the sample respond to B rather than to H, the oscillatory magnetization itself can produce a wave-shape distortion, which must be separated if the spin-dependent scattering contribution in $2\theta_1 - \theta_2$ and $3\theta_1 - \theta_3$ is to be resolved. This situation is simpler if the MI-induced harmonics M_r^{MI} can be shown to be much smaller than the Lifshitz-Kosevich (LK) harmonic content M_r^{LK}. A simple check for the presence of MI follows from work of Phillips and Gold.[34] The MI produce a second-harmonic contribution M_2^{MI} which is proportional to $(M_1/H)^2$. The resultant second-harmonic amplitude deviates (due to MI) from the phase of the LK component by an amount ψ, where we have

$$\psi = \tan^{-1}\left[\sin(\tfrac{3}{4}\pi)\Big/\left[\frac{M_2^{\mathrm{LK}}}{M_2^{\mathrm{MI}}} - \cos(\tfrac{3}{4}\pi)\right]\right]$$

$$= (2\theta_1 - \theta_2) \pm \tfrac{1}{4}\pi \ . \qquad (17)$$

The ratio $M_2^{\mathrm{MI}}/M_2^{\mathrm{LK}}$ is proportional to $T/H^{5/2}$, so that the worst-case condition is at low fields and high temperature. Since the scattering temperature drops out of the ratio in Eq. (17), a measurement of ψ in a pure crystal is a sufficient check on this effect in the alloys as well. The results of such relative phase-shift measurements on α and β hole orbits in both pure and alloy samples are shown in Fig. 6. The absence ($\pm 2°$) in the pure Rh crystal of a phase shift from the LK limit of $-45°$ (mod π) places an upper limit of 0.05 on the MI-to-LK amplitude ratio. (The phase shifts observed in the alloys are discussed in Sec. IV E.) As a check, the expected MI phase shift can be calculated once the g factor is known (Sec. IV D), using

$$\frac{M_2^{\mathrm{LK}}}{M_2^{\mathrm{MI}}} = \frac{2C_2}{(1-n)C_1^2}\left|\frac{\cos 2\pi S}{\cos^2 \pi S}\right|\frac{H^2}{8\pi^2 F} \ . \qquad (18)$$

The results[12] are consistent with the experimentally observed MI phase shift at $T = 1.2\,°\mathrm{K}$ in the pure metal (Fig. 6) being $0 \pm 2°$, and we are therefore justified in what follows in ignoring phase shifts due to MI for the X and L hole orbits. However, the situation in the larger electron orbit (Γ_{12}) is not so favorable, due to $F/H >> 1$ in Eq. (18). A numerical estimate indicates that the MI-induced harmonic M_2^{MI}

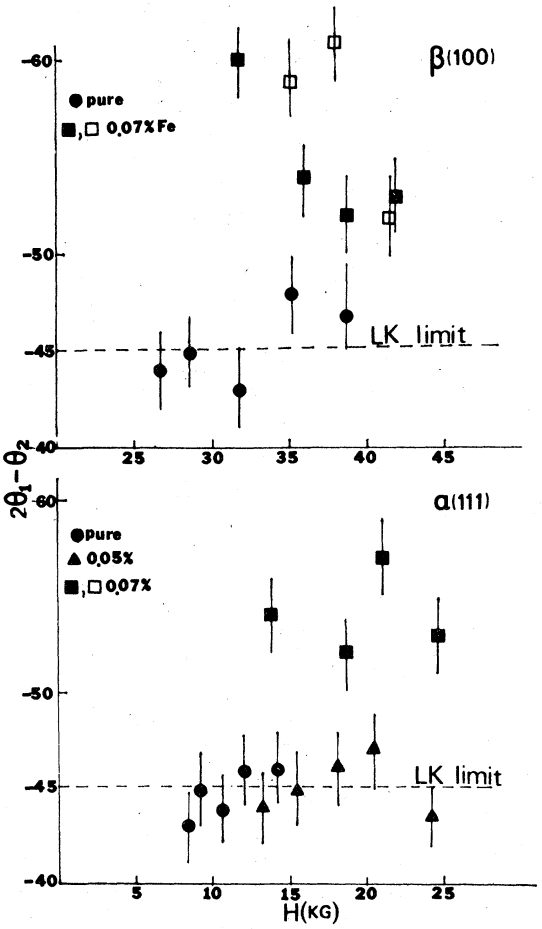

FIG. 6. Measurements of $2\theta_1 - \theta_2$ vs magnetic field in pure Rhodium (●) and Rhodium with Fe concentrations of 0.05 at.% (▲), 0.07 at.% (■) at $T = 1.2°$ K, and 0.07 at.% (□) at $T = 1.43\,°\mathrm{K}$.

dominates (~80% at $T = 1.2\,°\mathrm{K}$, $H = 80$ kG) in the second-harmonic content of these dHvA oscillations. For this reason, wave-shape analysis was not attempted for the Γ_{12} orbit.

C. Measurements of Dingle temperature on hole orbits in pure Rhodium

Measurements of Dingle temperature T_D on pure Rh crystals were made as a check on the "background" scattering (due to residual impurities and crystalline substructure) against which the alloy measurements may be compared. The results also provide a check on possible skin-depth errors in the higher harmonic detection used for wave-shape analysis. T_D could be determined either from the slope by plotting versus $1/H$, the function

$$\ln[(M_1 H/T)\sinh(k_B m^* T/H)] \ ,$$

TABLE V. Dingle temperature on hole orbits in pure Rh measured from different detection-frequency channels. (Units are K.)

	Field direction	Slope-Dingle-Temperature detection channels			Harmonic Dingle Temperature
Hole X_1	[100]	2ω	4ω	8ω	
		. . .	0.30 ±0.04	0.22 ±0.09	0.29 ± 0.04 (8ω channel)
Hole L	[111]	0.46 ±0.02	0.58 ±0.02	1.05 ±0.1	0.44 ± 0.1 (2ω and 4ω channels)

or from relative harmonic amplitudes at a single value of H shown here:

$$\ln\left(\frac{M_2^{LK}J_n'(\lambda)}{M_1^{LK}J_n'(2\lambda)}\frac{\sinh(\lambda_0 m^*T/H)}{(2)^{1/2}\sinh(2\lambda_0 m^*T/H)}\right) .$$

Here, M_2^{LK}/M_1^{LK} is the measured ratio of second harmonic to fundamental amplitude, and $J_n'(\lambda)/J_n'(2\lambda)$ is the ratio of *measured* modified Bessel functions. Since the skin-depth effects cancel in the harmonic ratio, the harmonic Dingle temperature serves as a double check on the slope Dingle measurements. Table V shows that the slope T_D for $\beta(100)$ orbits measured from 4ω and 8ω detection ($\omega = 17$ Hz) agrees well with the harmonic T_D measured using 8ω detection. However, the T_D measurements for $\alpha(111)$ orbits are frequency dependent, due to field-dependent resistance in the experimental field range. In order to avoid the skin-depth problem, the detection frequency was kept as low as possible, and harmonic T_D's were measured only from 2ω and 4ω detection channels.

D. *g* factor measurements on hole orbits in Rhodium

Since the contribution to the second harmonic of dHvA oscillations is small enough for MI to be neglected, the g factor in Rhodium could be calculated from

$$\gamma = \frac{M_2^{LK}J_n'(\lambda)/M_1^{LK}J_n'(2\lambda)\exp(\lambda_0 m^*T_D/H)}{\sinh(\lambda_0 m^*T/H)/(2)^{1/2}\sinh(2\lambda_0 m^*T/H)} . \quad (19)$$

Here,

$$\gamma \equiv |\cos 2\pi S/\cos\pi S| ,$$

and

$$S = g_c m^*/2 .$$

By plotting $|\cos(2\pi S)|$ and $\gamma|\cos(\pi S)|$ vs πS, the g factor could be calculated from the intersections. This method does not yield a unique value for the g factor, since any value of the parameter of the form $n \pm S$ (see Ref. 35) gives the same magnitude of $|\cos 2\pi S/\cos\pi S|$, where n is an integer. The input data and the two smallest corresponding values of g_c are shown in Table VI. To this extent, therefore, the choice of final g_c value must be guided by other considerations (for example, absolute phase measurements).[35]

TABLE VI. Input data for g_c calculation on $\alpha(111)$ and $\beta(100)$ orbits of Rhodium Fermi surface. The lack of field dependence justifies our neglect of magnetic-interaction corrections.

Direction	H (kG)	T_D (°K)	$\left(\frac{M_2^{LK}}{M_1^{LK}}\right)^{obs}\left(\frac{J_n'(\lambda_1)}{J_n'(2\lambda_1)}\right)$	$\left\|\frac{\cos 2\pi S}{\cos\pi S}\right\|$	πS	g_c
$\alpha(111)$	9.89	$0.46^{+0.02}_{-0.1}$	0.0275	1.36	1.11, 2.04	$5.13^{+0.03}_{-0.25}, 9.48^{+0.03}_{-0.25}$
	14.67	$0.46^{+0.02}_{-0.1}$	0.088	1.30	1.10, 2.05	
$\beta(100)$	29.6	0.30 ± 0.04	0.064	2.55	1.25, 1.90	1.78 ± 0.01, 2.67 ± 0.01
	38.2	0.30 ± 0.04	0.144	2.79	1.27, 1.88	

E. Dingle-temperature and exchange-field measurements on $\alpha(111)$, $\beta(100)$, and $\delta(111)$ orbits in RhFe

In the presence of polarized impurity spin, spin-dependent scattering could produce a phase shift $\Delta\theta_r$ (illustrated in Fig. 1) from the LK phase. Since this can alter the resultant amplitude, errors in conventional (slope) Dingle temperature can result. However, measurements of $2\theta_1-\theta_2$ on $\alpha(111)$ and $\beta(100)$ in RhFe (0.05- and 0.07-at.% Fe) (Fig. 6) show phase shifts which are small enough and have a small enough field dependence that the slope Dingle temperature versus $1/H$ and point Dingle temperature at a single H are equally valid without a correction factor for the two spin components. A summary of measurements on scattering rate in several RhFe alloys as a function of temperature on $\alpha(111)$, $\beta(100)$, and $\delta(111)$ orbits is given in Tables VII and VIII.

Figure 7 shows that the scattering temperatures T_D on $\alpha(111)$ and $\beta(100)$ orbits in Rh–0.05-at.% Fe display a weak temperature dependence. But on $\delta(111)$ orbits, $T_D(T)$ displays a strong temperature dependence whose slope is a factor of 4 larger than observed in resistivity measurements *on samples cut from the same crystal.*[36] Figures 8 and 9 show that T_D on $\alpha(111)$ and $\beta(100)$ orbits display a stronger temperature dependence in a more concentrated sample, and that T_D on $\beta(100)$ orbits displays a larger temperature dependence than that of $\alpha(111)$ orbits in the same alloy.

Since the assumption was valid that T_D (slope) $\simeq\bar{T}_D$ ($\uparrow\downarrow$ average) on $\alpha(111)$ and $\beta(100)$ orbits in the experimental field and temperature range, ΔT_D and H_{ex} could be calculated[9] from two observable quantities, $(R_2/R_1)^{obs}$ and $2\theta_1-\theta_2$,[9]

$$\left(\frac{R_2}{R_1}\right)^{obs}=\frac{(C_2D/C_1)[E^{-2}+E^2+2\cos(2\pi S')]^{1/2}}{E^{-4}+E^4+2\cos(4\pi S')]^{1/2}}\ , \tag{20}$$

$$\Delta(2\theta_1-\theta_2)=2\tan^{-1}[\tan(\pi S')(1-E^2)/(1+E^2)]-\tan^{-1}[\tan(2\pi S')(1-E^4)/(1+E^4)]\ , \tag{21}$$

where, $(R_2/R_1)^{obs}=[M_2^{LK}J_n'(\lambda)/M_1^{LK}J_n'(2\lambda)]$ is the ratio of second- and first-harmonic amplitude and $S'=g_c'm^*/2m_0$. Here, g_c' is an effective g factor which is modified by the exchange-energy H_{ex} coupling conduction electrons to the impurity[37]

$$g'=g-H_{ex}/\mu_B H\ , \tag{22}$$

and $\Delta(2\theta_1-\theta_2)=(2\theta_1-\theta_2)_{SDS}-(2\theta_1-\theta_2)_{LK}$ is the Fe-induced phase shift from the LK limit of $-45°$.[38] Various π phase shifts in the experimental system introduce a π modularity in $2\theta_1-\theta_2$ which is difficult to eliminate.[9] However, comparison with pure-Rh data taken under the same condition, allowed $\Delta(2\theta_1-\theta_2)$ to be determined modulo 2π. The result-

TABLE VII. Summary of the scattering rates on $\alpha(111)$, $\beta(100)$, and $\delta(111)$ in Rhodium with Fe concentration 0.05%.

Orbit and Direction	Temperature (°K)	T_D (°K)	dT_D/dT
	1.18	1.13 ± 0.02	
α orbit	1.74	1.18 ± 0.03	
	2.47	1.17 ± 0.02	(0.04 ± 0.02)
[111]	3.36	1.12 ± 0.02	
	4.20	1.26 ± 0.04	
	1.19	0.78 ± 0.09	
β orbit	1.64	0.88 ± 0.09	
[100]	2.89	0.86 ± 0.04	(0.04 ± 0.02)
	4.20	0.93 ± 0.04	
	1.17	$1.36^{+0.02}_{-0.2}$	
δ orbit	1.40	$1.43^{+0.07}_{-0.2}$	(0.40 ± 0.08)
[111]	1.61	$1.49^{+0.07}_{-0.02}$	
	1.81	$1.67^{+0.12}_{-0.2}$	

TABLE VIII. Summary of scattering rates on $\alpha(111)$ and $\beta(100)$ orbits in Rhodium with Fe concentration 0.07, 0.11, and 0.21%.

Concentration	Direction	Temperature (°K)	T_D (°K)	$\frac{dT_D}{dT}$
	α[111]	1.13	1.47 ± 0.03	. . .
	β[100]	1.17	1.02 ± 0.03	
		1.43	1.04 ± 0.05	
0.07%		2.13	1.26 ± 0.09	(0.24 ± 0.02)
		2.42	1.33 ± 0.07	
		3.06	1.44 ± 0.13	
	α[111]	1.12	1.91 ± 0.04	
		2.12	1.95 ± 0.04	
0.11%		2.98	1.97 ± 0.01	(0.09 ± 0.05)
		3.60	2.17 ± 0.03	
		4.20	2.34 ± 0.33	
	β[100]	1.14	1.31 ± 0.1	
		1.60	1.33 ± 0.3	(0.31 ± 0.13)
		2.32	1.61 ± 0.06	
	α[111]	1.20	3.87 ± 0.21	. . .
		1.61	3.17 ± 0.62	
0.21%				
	β[100]	1.17	2.60 ± 0.13	. . .
		2.25	2.64 ± 0.30	

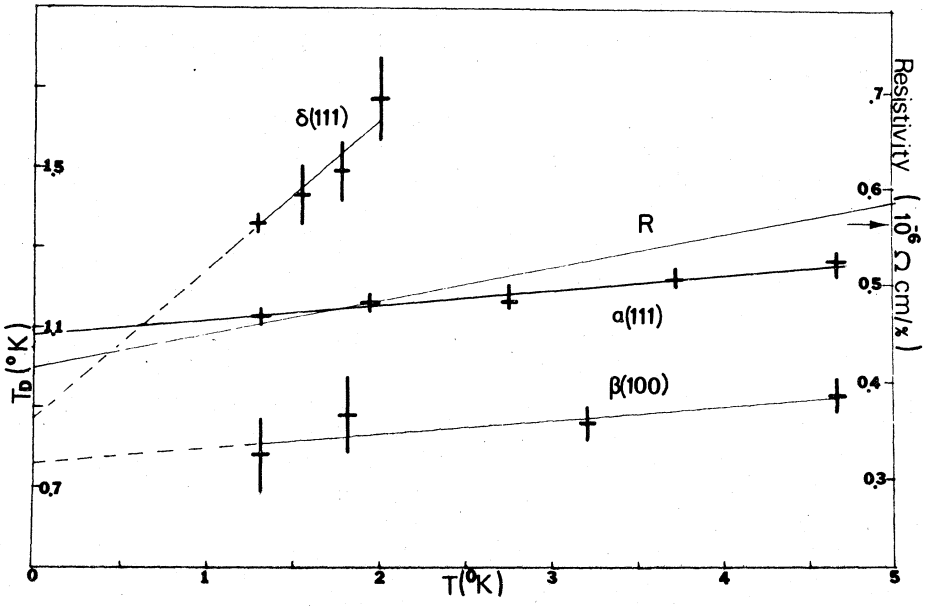

FIG. 7. Comparison of temperature dependence of scattering on $\delta(111)$, $\beta(100)$, and $\alpha(111)$ orbits with resistivity in Rh with an Fe concentration of 0.05 at.%.

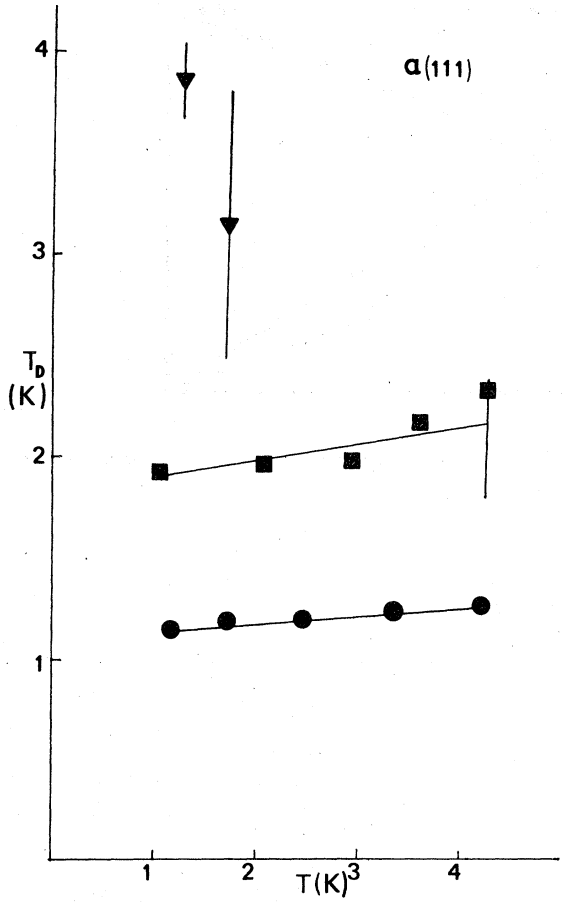

FIG. 8. Temperature dependence of the scattering rate of $\alpha(111)$ orbits in Rh with Fe concentrations of 0.05 at.% (●), 0.11 at.% (■), and 0.21 at.% (▼) assuming $m^*/m_0 = 0.137$.

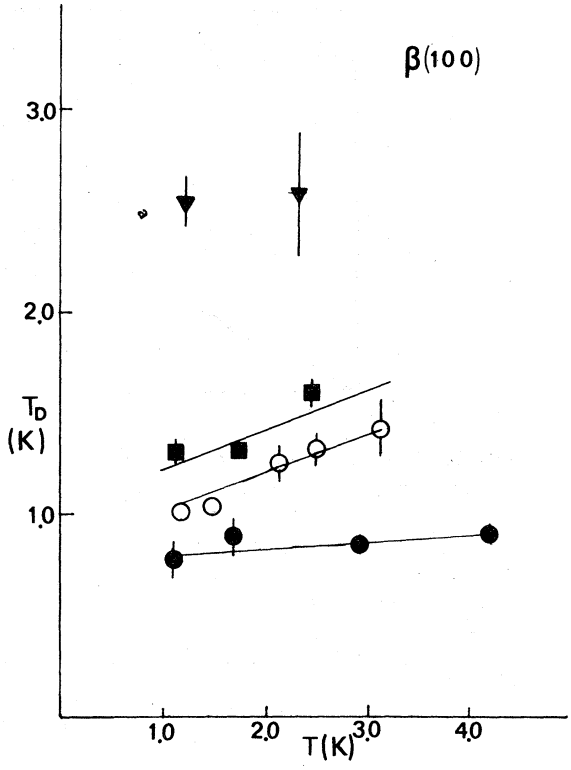

FIG. 9. Temperature dependence of scattering rates of $\beta(100)$ orbits in Rh with Fe concentrations of 0.05 at.% (●), 0.07 at.% (○), 0.11 at.% (■), and 0.21 at.% (▼), assuming $m^* = 0.453$.

ing Fe-induced phase shift is shown in Fig. 6.

Since the Eqs. (20) and (21) are coupled and transcendental, ΔT_D and H_{ex} were calculated graphically from observables R_2/R_1 and $\Delta(2\theta_1 - \theta_2)$, that is, from the intersections of

$$\left(\frac{C_1}{DC_2}\right)\left(\frac{R_2}{R_1}\right)^{\text{obs}} [E^{-4} + E^4 + 2\cos(4\pi S')]^{1/2}$$

and

$$[E^{-2} + E^2 + 2\cos(2\pi S')]^{1/2} \ ,$$

which is Eq. (20). This makes use of the quantity E which was first calculated numerically as a function of S' from Eq. (21) using the observed $\Delta(2\theta_1 - \theta_2)$. An example of a graphical solution is shown in Fig. 10. Note that the S' values are fortuitously in a region which leads to a large shift in the observables for a small shift in S', leading to an accurate determination of S' and hence g'. The input data and results of calculation are shown in Tables IX and X. Only data on $\alpha(100)$ and $\beta(100)$ orbits with Fe concentrations 0.05 and 0.07 at.% at $T = 1.2$ °K had enough second-harmonic amplitudes to be analyzed. The $\delta(111)$ orbit with its larger effective mass ($1.99 m_0$) had a harmonic signal too weak for a reliable waveshape analysis.

Table X shows that no spin-dependent scattering was observed, but a g shift of ~8% (antiferromagnetic) was found on $\alpha(111)$ orbits in Rh–0.05-at.% Fe [assuming the smallest g value obtainable from the measured $\cos(\pi g_c m^*/2)$]. A shift of ~10% (antiferromagnetic) was observed on $\alpha(111)$ and $\beta(100)$ orbits in Rh–0.07-at.% Fe. The impurity self-energy terms $\mathrm{Im}\Sigma\uparrow$, $\mathrm{Im}\Sigma\uparrow$, and $\mathrm{Re}(\Sigma\uparrow - \Sigma\downarrow)$ are also indicated in Table X, calculated from Eq. (1) using experimental values of H_{ex} and ΔT_D. Figure 11 shows that the exchange field on $\alpha(111)$ and $\beta(100)$ orbits displays a weak field dependence. The magnitude of H_{ex} seen by the conduction electrons is considerably smaller than that of the Mössbauer measurements,[39] which give a value of H_{ex} seen at the nucleus of ~0.08 kG/ppm at $H = 20$ kG, $T = 1.2$ K.

The observed small spin-dependent scattering and small field dependence of $\cos(\pi S')$ on both orbits

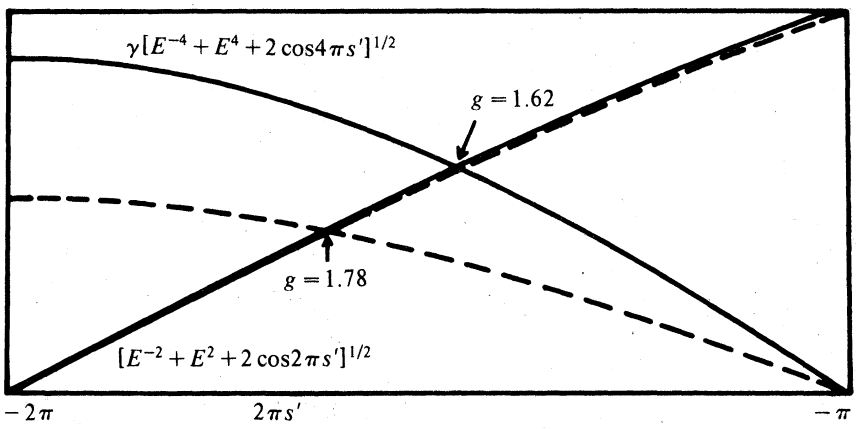

FIG. 10. Graphical solution for the g factor of the $\beta(100)$ orbit illustrating the substantial size of the g shift between pure Rh (dashed curve) and Rh–0.07-at.% Fe (solid curve).

TABLE IX. Input data for g-factor calculation on $\alpha(111)$ and $\beta(100)$ orbits of RhFe.

Field direction	Concentration (at.%)	H (kG)	$\bar{T}_D$ (°K)	$\Delta(2\theta_1-\theta_2)$	γ[a]	$\pi S'$	g_c[b]
	0.05%	12.57	1.06 ± 0.02	0° ± 2°	0.83	1.01, 2.13	4.69 ± 0.1 9.89 ± 0.1
		17.69	1.06 ± 0.02	0° ± 2°	0.83	1.01, 2.13	4.69 ± 0.1 9.89 ± 0.1
α[111]							
	0.07%	21.40	1.41 ± 0.03	−8° ± 2°	0.66	0.98, 2.16	4.55 ± 0.1 10.03 ± 0.1
		24.50	1.41 ± 0.03	−9° ± 2°	0.78	1.00, 2.14	4.65 ± 0.1 9.95 ± 0.1
		42.28	1.02 ± 0.03	−9.2° ± 2°	1.63	1.15, 1.99	
β[100]		36.16	1.02 ± 0.03	−9.7° ± 2°	1.68	1.16, 1.98	1.62 ± 0.03 2.80 ± 0.03
	0.07%	32.83	1.02 ± 0.03	−15° ± 2°	1.64	1.15, 1.99	
		29.94	1.02 ± 0.03	−22° ± 2°	1.62	1.15, 1.99	

[a] $\gamma=[E^{-4}+E^{4}+2\cos(4\pi S')]^{1/2}/[E^{-2}+E^{2}+2\cos(2\pi S')]^{1/2}$.

[b] Only the two smallest possible values of g_c are tabulated.

TABLE X. Values of g_c', H_{ex}, ΔT_D, $\mathrm{Im}(\Sigma_\downarrow)$, $\mathrm{Im}(\Sigma_\uparrow)$, and $\mathrm{Re}(\Sigma_\uparrow-\Sigma_\downarrow)$ on $\alpha(111)$ and $\beta(100)$ orbits in RhFe.

Direction	H (kG)	Concentration (at.%)	g_c'[a]	H_{ex} (kG)	H_{ex} (10^{-3} kG/ppm)	ΔT_D (°K)	$\mathrm{Im}(\Sigma_\downarrow)$ $\times(10^{-4}$ eV)	$\mathrm{Im}(\Sigma_\uparrow)$ $\times(10^{-4}$ eV)	$\mathrm{Re}(\Sigma_\uparrow-\Sigma_\downarrow)$ $\times(10^{-5}$ eV)
	12.57		4.69 ± 0.05	(6^{+1}_{-4})	(11^{+2}_{-8})				$(3.4^{+0.6}_{-2.5})$
		0.05%				0.00 ± 0.01	−2.8	−2.8	
	17.69		4.69 ± 0.05	(8^{+2}_{-6})	(16^{+4}_{-12})				$(4.9^{+1.7}_{-3.7})$
α[111]									
	21.20		4.55 ± 0.05	(12^{+2}_{-6})	(17^{-3}_{-9})				(8^{+1}_{-4})
		0.07%				0.02 ± 0.02	−3.9	−3.8	
	24.50		4.65 ± 0.05	(12^{+2}_{-6})	(17^{+3}_{-9})				(8^{+1}_{-4})
	42.28			6.7 ± 1.7	9.6 ± 2.4	0.01 ± 0.01			(4.2 ± 1)
	36.16			5.8 ± 1.7	8.3 ± 2.4	0.01 ± 0.01			(3.6 ± 1)
β[100]		0.07%	1.62 ± 0.03				−2.8	−2.8	
	32.83			5.2 ± 1.7	7.5 ± 2.4	0.02 ± 0.01			(3.3 ± 1)
	29.94			5.2 ± 1.7	7.5 ± 2.4	0.03 ± 0.01			(3.3 ± 1)

[a] The g factor on $\alpha(111)$ and $\beta(100)$ orbits in pure Rhodium is $5.13^{+0.03}_{-0.25}$ and 1.78 ± 0.01, respectively.

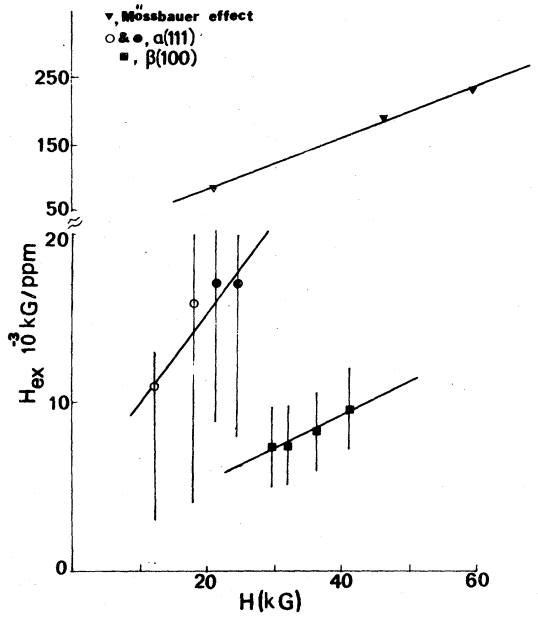

FIG. 11. Measured exchange field (kG/ppm) on $\beta(100)$ orbits in Rh with 0.07-at.% Fe (■) and $\alpha(111)$ orbits with 0.05-at.% (○) and 0.07-at.% (●) Fe as a function of magnetic field, compared to the Mössbauer effect (▼).

confirm the assumption, used above, that the slope T_D is an adequate measure of the average scattering.

F. Phase-shift analysis of Fe-impurity scattering in Rh at $T=0$ K

The impurity scattering rate at E_F can be characterized by scattering phase shifts only if the scattering is elastic.[15] Since the experimental measurements show that the Fe-induced exchange field (kG/ppm) and spin-dependent scattering on the orbits of $\alpha(111)$ and $\beta(100)$ in RhFe are relatively small (smaller by one order of magnitude than that of CuFe, for example[2]), non-spin-flip scattering appears to dominate on both these sheets of FS and a phase-shift model appears appropriate. The orbit-independent parameters $\mathrm{Im}S_L$ can be calculated using the set of observed scattering rates $\bar{T}_{Di}$ for the i th orbit[17] and the calculated symmetry information of Table II.

$$\pi k_B \bar{T}_{Di} = \frac{\hbar^2 c}{2\pi m^*} \sum_L \mathrm{Im}S_L \left(\frac{\partial A_i}{\partial \eta_L} \right)_{E_F} . \tag{23}$$

From S_l, the set of phase shifts can be determined using Eq. (5b). This is done first using data extrapolated to $T=0$ °K to obtain zero-temperature phase shifts, the interpretation of which is *model independent.* Then the observed temperature dependences, together with information on the exchange energy and spin-dependent scattering, will be used to explore the origin of the unusual temperature dependence of the resistivity.

If the host metal has little influence on the wave function inside the impurity cell [i.e., the backscattering coefficient $A_L \simeq 1$ in Eq. (5b)], the difference between the impurity and host-metal phase shifts (scattering phase shifts) for p and d waves found using the above procedure are

$$\Delta\eta_1 = 0.31 \pm 0.02 \text{ rad} \quad (S_1 = 0.085) ,$$

$$\Delta\eta_2 = 0.21 \pm 0.02 \text{ rad} \quad (S_2 = 0.043) .$$

These were obtained using X and L hole-orbit data (0.05-at.% Fe) only. As a check, these numbers may be used to calculate $T_D(0)$ for the $\delta(111)$ (d wave only). The results are consistent since we have

$$T_{D\delta}(0) = 0.64 \pm 0.15 \text{ K (calculated)}$$

$$= 0.86^{+0.1}_{-0.2} \text{ K (observed)} .$$

Since the values of $(\partial A/\partial n_0)E_F$ on all these orbits are near zero (lack of s-wave symmetry), the value of $\mathrm{Im}S_0$ could not be determined from Eq. (22). In view of the d-like nature of the Fe impurity, it is not expected to be important.

G. Temperature-dependent scattering rates

The dominant feature shown in Fig. 7 is that the temperature dependence of scattering rate measured on $\alpha(111)$ and $\beta(100)$ orbits is much smaller than the resistivity measured from an adjacent sample, although the temperature-dependent scattering rate on the $\delta(111)$ orbits is larger than that of the resistivity. In higher concentration alloys no $\delta(111)$-orbit data is available because of its large effective mass, and $\alpha(111)$ and $\beta(100)$ orbits (Figs. 8 and 9) appear to be more strongly T dependent (but do not scale linearly with concentration), with $T_{D\alpha}^{-1} dT_{D\alpha}/dT \lesssim T_{D\beta}^{-1} dT_{D\beta}/dT$. This is the first time that a temperature-dependent scattering has been observed directly on specific Fermi-surface sheets in a transition-metal alloy. Since the smaller α and β sheets contribute relatively little (18%) to the conductivity, as shown on Table XI, the absence of a temperature dependence is first of all not inconsistent with the resistivity, which averages contributions for all sheets. Secondly, the fact that these sheets contain admixtures of p waves shows qualitatively that the origin of the large positive dR/dT is connected with the d-wave part of the host, hence the d-scattering phase shift. The puzzle is that the slope for the $\delta(111)$ orbits is so large. To the extent that resistivity scattering and dHvA scattering follow analogous phase-shift models, and given that the majority carriers are, like this one, d-like, one would expect rather similar behavior of $R(T)$ and $T_{D\delta}(T)$.

TABLE XI. Scattering anisotropy expressed as scattering temperature X and % contribution to conductivity in Rhodium–0.05-at.% Fe at $T=1.2\,^{\circ}\mathrm{K}$.

FS sheet	m^*	X (°K)	Symmetry	% contribution to conductivity
L_3 holes (α orbit)	0.137	1.06	p-d mixture	5
X_5 holes (β orbit)	0.453	0.78	p-d mixture more d-like	13
Γ_{12} electrons (δ orbit)	1.99	1.36	d-like	28
X_2 holes (γ orbit)	1.2	~1.0[a]	d-like	10
$\Gamma_{25'}$ electrons	4.0[b] (est)	~1.0[a] (est)	d-like	44

[a]In view of the d-like nature of the conduction electron on this sheet of Fermi surface, the scattering rate is expected to be similar to δ orbits.
[b]Anderson's energy-band calculation (Ref. 26).

Unfortunately, direct scattering measurements on the largest sheet has not yet been possible (because of the large m^*). However, from the symmetry-character calculation (refer to Table II), it too is dominated by d character. We now explore the implications of the anisotropy in temperature-dependent scattering for the origin of the magnetic-impurity behavior in RhFe.

a. In Knapp's two-band model,[3] d-like electrons couple to the Fe-impurity spin via an antiferromagnetic interaction at low temperatures and screen the Fe magnetic moments. The current is carried by conduction electrons and is dominated by s electrons. These are scattered from localized moments which are increasingly screened as T is lowered, leading to a decrease in the observed resistance. However, if true, the scattering of d-like electrons would increase as the temperature was lowered. Since most of the current is carried by d electrons (Table XI), whose temperature dependence of scattering is found to be positive (Fig. 7) rather than negative, this explanation can be rejected.

b. Based on the Kondo Model,[4] a potential scattering phase shift modifies the coefficient of the $\ln T$ term in the s-d expression for the resistivity by a factor $\cos 2\Phi_L$. Thus, if any of the Φ_L, the Friedel phase shifts, are greater than $\frac{1}{4}\pi$, the slope of the $\ln T$ term in the resistivity will change sign from the usual (negative) Kondo effect. Here, the Φ_L are defined through[17]

$$S_L = I_L^{-1} \sin\Phi_L \, e^{i\Phi_L} \ ,$$

where

$$I_L = \text{const} \int_{\text{FS}} dk/d\eta_L \, dS_k \ .$$

Since the Φ_L are a measure of the total charge difference localized on the impurity site, they are preferable to the impurity-host phase-shift differences $\Delta\eta_L$ [Eq. (5b)] as a measure of Kondo's potential scattering term. Although I_L has not been calculated, involving an integral over the entire FS, much of which has not yet been mapped, a qualitative estimate may be made by noting the I_L and $\partial A/\partial\eta_L$ are similar quantities

$$\sin^2\Phi_L = I_L \, \mathrm{Im} S_L \propto (\partial A/\partial\eta_L) \, \mathrm{Im} S_L \ .$$

Taking the $\Gamma_{25'}$ sheet as a sample of the FS integral I_L, the results in Table II imply that

$$\Phi_1 \sim (0.13)^{1/2}\Delta\eta_1 = 0.11 \text{ rad} \ ,$$

$$\Phi_2 \sim (3.5)^{1/2}\Delta\eta_2 = 0.39 \text{ rad} \ ,$$

using values of $\Delta\eta_L$ from the $T=0$ extrapolation (i.e., potential scattering) of the previous section. The fact that the $\Delta\eta_L$ are comparable to each other, while the Φ_L are dominated by Φ_2, is evidence that the Fe impurity is *also* near a d-wave resonance (Fig. 4), i.e., most of the impurity charge density is d-like. However, the values in this estimate still fall short of

the value $\pi/4 = 0.78$ rad, at which the Kondo mechanism is applicable.

c. Based on the Anderson model, Shiba[10] and Nagasawa[5] related the temperature dependence of the non-spin-flip scattering to the temperature dependence of the impurity magnetic moment. The scattering rate can be related to the scattering phase shifts as follows:

$$\pi k_B \bar{T}_D = \frac{\hbar^2 c}{2\pi m^*}\left[\sin^2\Delta\eta_0\left(\frac{\partial A}{\partial \eta_0}\right)_{E_F} + \sin^2\Delta\eta_1\left(\frac{\partial A}{\partial \eta_1}\right)_{E_F} + [\tfrac{1}{2}\sin^2\eta_2^{\uparrow}(T) + \tfrac{1}{2}\sin^2\eta_2^{\downarrow}(T)]\left(\frac{\partial A}{\partial \eta_2}\right)_{E_F}\right] . \tag{24}$$

It is convenient to break the d-wave phase shift into two spin components, and transform those two components into an average $\Delta\eta_2(0)$ and a difference term $\eta_2'(T)$

$$\eta_2^{\uparrow\downarrow}(T) = \Delta\eta_2(0) \pm \eta_2'(T) \quad , \quad \Delta\eta_2(0) = \tfrac{1}{2}[\Delta\eta_2^{\uparrow}(0) + \Delta\eta_2^{\downarrow}(0)] = \Delta\eta_2^{\uparrow}(0) = \Delta\eta_2^{\downarrow}(0) \quad ,$$
$$\eta_2'(T) = \tfrac{1}{2}[\eta_2^{\uparrow}(T) - \eta_2^{\downarrow}(T)] \quad , \tag{25}$$

where $\eta_2^{\uparrow}(T)$ and $\eta_2^{\downarrow}(T)$ are the d-wave scattering phase shifts for spin-up and -down electrons, respectively. $\Delta\eta_2(0)$ is the d-wave *potential* scattering phase-shift difference between impurity and host. Using this, Eq. (24) becomes

$$\pi k_B \bar{T}_D = \frac{\hbar^2 c}{2\pi m^*}\left[\sin^2\Delta\eta_0\left(\frac{\partial A}{\partial \eta_0}\right)_{E_F} + \sin^2\Delta\eta_1\left(\frac{\partial A}{\partial \eta_1}\right)_{E_F} + \sin^2\Delta\eta_2(0)\left(\frac{\partial A}{\partial \eta_2}\right)_{E_F} + \cos 2\Delta\eta_2(0)\sin^2\eta_2'(T)\left(\frac{\partial A}{\partial \eta_2}\right)_{E_F}\right] . \tag{26}$$

Thus, the scattering rate is expressed as the sum of temperature-independent and temperature-dependent terms. The increment of the scattering rate on the i th orbit at finite temperature T compared to $T = 0\,^\circ\mathrm{K}$ is expressed as follows:

$$\Delta T_D(T) \equiv T_D(T) - T_{Di}(0) = \left(\frac{\hbar^2 c}{2\pi^2 m_i^* k_B}\right)\cos 2\Delta\eta_2(0)\left(\frac{\partial A}{\partial \eta_2}\right)_{E_F}\sin^2\eta_2'(T) \quad . \tag{27}$$

The problem is that the only orbit-dependent term in Eq. (27) in this model is $(\partial A/\partial\eta_2)/m_i^*$, and the calculated orbital differences (Table II) are not large enough to explain the very different slopes observed, for example, in Fig. 7. A comparison of the fraction of d-wave nature $(\partial A/\partial\eta_2/\sum \partial A/\partial\eta_l)$ calculated from Table II with an average of the slopes (scaled to concentration) $c^{-1}(dT_D/dT)$ from Tables VII and VIII (Figs. 7–9) for the different orbits is shown in Fig. 12. It is clear from this that the temperature dependence of scattering rate grows at a rate significantly faster than the percentage of d-wave character in the host, in contrast to experiments in the noble metals. Note that this discrepancy is not due to uncertainties in m^* (see Table IV). The discrepancies between the experimental results and the phase-shift analysis of the temperature dependence of scattering rate suggest either that *orbital-dependent* phase shifts are required, or that the explanation must go beyond the Anderson model phase-shift picture.

d. By analogy with the temperature dependence of the resistivity due to LSF *proposed by Rivier and Zlatic,*[40,41] the orbital variation in the temperature dependence of scattering rate might be accounted for by the following argument. The difference in the temperature dependence of the scattering rate between $\delta(111)$ and $\beta(100)$ or $\alpha(111)$ orbits lies in the coupling between the conduction electrons and LSF. On $\delta(111)$ orbits, the conduction electrons and Fe-impurity spin (with the same d-like symmetry) are strongly coupled by J and interact with the LSF directly. However, on $\alpha(111)$ and $\beta(100)$ orbits, conduction electrons are of mixed p-d symmetry, and may have to first tunnel into an intermediate state where LSF takes place before being scattered. As a result, the scattering temperature of different orbits may display a qualitatively different temperature dependence. However, the calculation of scattering rate in the LSF model has been done only for *transport* measurements such as resistivity. It would be of interest to extend the formula-

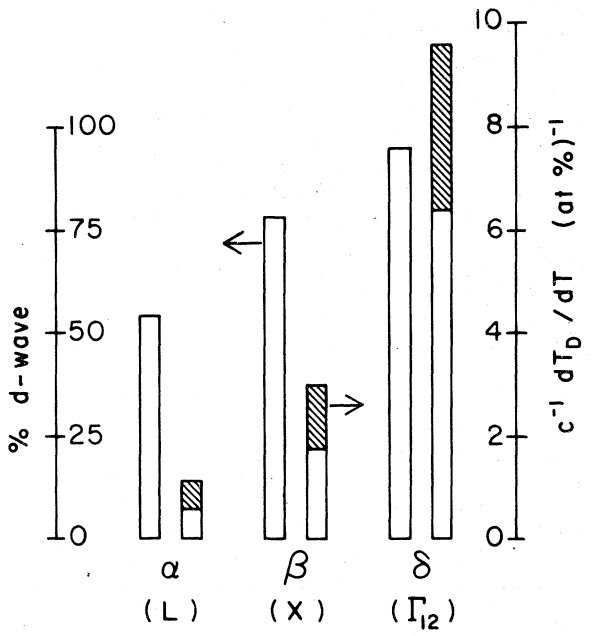

FIG. 12. Comparison of the percentage of *d*-wave character (as defined in the text) with the temperature dependence (scaled to concentration) of the scattering rate for three FS orbits in RhFe.

tion to deal with the scattering rate in an equilibrium property such as the dHvA effect, for host conduction electrons of mixed symmetry.

IV. CONCLUSIONS

Waveform analysis of the dHvA signal on $\alpha(111)$ and $\beta(100)$ orbits in 0.05-at.% and 0.07-at.% Fe in Rh at $T=1.2\,^{\circ}\mathrm{K}$ have been made to deduce the spin-dependent scattering and the exchange field due to the impurity spin. Little spin-dependent scattering was observed, but a g shift of -8% from pure Rhodium (antiferromagnetic) was found on $\alpha(111)$ orbits with 0.05-at.% Fe. A g shift of -10% from pure Rhodium (antiferromagnetic) was also observed on both $\alpha(111)$ and $\beta(100)$ orbits with 0.07-at.% Fe. The evidence that the exchange coupling in RhFe is antiferromagnetic in sign is consistent with Mössbauer and susceptibility[42] measurements. The small (2%) observed spin-dependent scattering and the small exchange field (0.01 kG/ppm) are consistent with the spin-fluctuation temperature $T_{sf}\sim 2\,^{\circ}\mathrm{K}$ given by the resistivity measurements.[36]

Results of conventional slope-Dingle-temperature measurements with 0.05-at.% Fe in Rh display a temperature dependence which varies with orbit, with the most *d*-like orbits showing the largest temperature dependence. This proves that the large dR/dT is connected with the *d*-wave part of the host.

Knapp's two-band model[3] and Kondo's idea[4] of simultaneous spin and potential scattering, proposed for the explanation of resistivity anomaly in RhFe, have been ruled out because of the observed positive temperature dependence of scattering rate on *d*-like $\delta(111)$ orbits, and because of the calculated small potential scattering phase shift, respectively.

It was demonstrated that phase-shift analysis of the scattering rate in terms of a temperature-dependent occupation of the spin-up (-down) impurity band may not be strictly valid for *all* the sheets of the Fermi surface. However, since the conductivity and charge screening take place in the same band on $\delta(111)$ orbits, one would expect the analysis of the scattering rate in terms of phase shifts to be adequate. Since the sheets of Fermi surface in Rhodium which contribute $\sim 80\%$ of the conductivity are *d*-like, one would expect $R(T)$ and $T_{D\delta}(T)$ to follow an analogous phase-shift model. The puzzle is that the slope of $R(T)$ is a factor of 4 smaller than that of $T_{D\delta}(T)$. Since the $T_{D\delta}(T)$ was measured over a very narrow range of T, the fitted straight line gives somewhat uncertain parameters, and an extension to a wider temperature range ($0.3-1.8\,^{\circ}\mathrm{K}$) is desirable, and is underway.

A direct comparison of our work with the LSF model must await a formulation of orbitally averaged lifetimes due to LSF, to obtain expressions for the quantities measured in dHvA experiments.

ACKNOWLEDGMENTS

This project was begun while one of us (RJH) was a sabatical-year visitor at the Bell Laboratories, and all of the crystal growth and chemical analyses were performed at that institution. We especially wish to thank W. A. Reed for his efforts as a facilitator during that fruitful visit. All of the measurements and the APW calculations reported here were done at the University of Oregon, with the support of the NSF (Grant No. DMR 76-14878). We thank Peter Coleridge for helpful advice and sample computer programs dealing with off-symmetry point APW calculations, and L. F. Matthiess for helpful discussions on eliciting wave-function symmetry from APW energy bands. We thank D. H. Lowndes for several weeks use of his 80-kG solenoid system for some of the measurements, T. Kometani for chemical analysis, and Sven Hornfeldt for providing us with his effective-mass values prior to publication.

*Present address: Electronic Device Div., Rockwell Intern., Anaheim, Calif. 92803.
[1]B. R. Coles, Phys. Lett. 8, 243 (1964).
[2]R. L. Rusby, J. Phys. F 4, 1265 (1974).
[3]G. S. Knapp, Phys. Lett A 25, 114 (1967).
[4]J. Kondo, Phys. Rev. 169, 437 (1968).
[5]H. Nagasawa, Solid State Commun. 10, 33 (1972).
[6]A. B. Kaiser and S. Doniach, Int. J. Magn. 1, 11 (1970).
[7]A. V. Gold, *Solid State Physics, Electrons in Metals,* edited by J. F. Cochran and R. R. Hearing (Gordon and Breach, New York, 1968) Vol. 1.
[8]H. G. Alles, R. J. Higgins, D. H. Lowndes, Phys. Rev. Lett. 30, 705 (1973).
[9]H. G. Alles, R. J. Higgins, Phys. Rev. B 9, 158 (1974).
[10]H. Shiba, Prog. Theor. Phys. 50, 1797 (1973).
[11]R. J. Higgins *et al., Proceedings of the 14th International Conference on Low Temperature Physics* (North-Holland, Amsterdam, 1975), Vol. III, p. 146.
[12]L. S. Cheng, Ph.D. thesis, University of Oregon, 1977. Available on microfilm from University Microfilms, Ann Arbor, Mich. (Dissertation DBJ 77-19332).
[13]D. H. Lowndes and Yun Chung, Phys. Cond. Matter 19, 285 (1975).
[14]R. Harris, B. G. Mulimani, and J. O. Ström-Olsen, J. Phys. F 5, 1910 (1975).
[15]J. R. Schrieffer, J. Appl. Phys. 38, 1143 (1967).
[16]P. T. Coleridge, G. B. Scott, I. M. Templeton, Can. J. Phys. 50, 1999 (1972).
[17]P. T. Coleridge, N. A. W. Holzwarth, and M. J. G. Lee, Phys. Rev. B 10, 1213 (1974); N. A. W. Holzwarth, Phys. Rev. B 11, 3718 (1975).
[18]This point of view, which is common in the magnetic-impurity literature (e.g., Ref. 6) is weakened by dHvA measurements in noble-metal hosts (e.g., Ref. 19) which show that the scattering rate from a $3d$ transition-metal impurity is proportional to the d character of the host, even in such classic Kondo systems.
[19]P. A. Wolff, Phys. Rev. 124, 1030 (1961).
[20]M. L. G. Lee, Phys. Rev. 178, 953 (1969); 187, 901 (1969); Phys. Rev. Lett. 26, 501 (1971).
[21]J. C. Shaw, J. B. Ketterson, and L. R. Windmiller, Phys. Rev. B 5, 3894 (1972).
[22]J. B. Ketterson, D. D. Koelling, J. C. Shaw, and L. R. Windmiller, Phys. Rev. B 11, 1447 (1975).
[23]D. A. Liberman and D. T. Cromer, Computer Phys. Commun. 2, 107 (1971).
[24]T. L. Loucks, *Augmented Plane Wave Method* (Benjamin, New York, 1967).
[25]O. K. Andersen, Phys. Rev. B 2, 883 (1970).
[26]Orbit Tracing: J. B. Ketterson, F. M. Mueller, and L. R. Windmiller, Phys. Rev. 186, 656 (1969). Areas: P. Coleridge, private communication.
[27]P. T. Coleridge, Proc. R. Soc. London Ser. A 295, 476 (1966).
[28]L. F. Mattheiss (private communication).
[29]R. W. Stark and L. R. Windmiller, Cryogenics 8, 272 (1968).
[30]L. R. Windmiller and J. B. Ketterson, Rev. Sci. Instrum. 39, 1672 (1968).
[31]H. G. Alles and R. J. Higgins, Rev. Sci. Instrum. 46, 963 (1975).
[32]H. G. Alles and R. J. Higgins, Rev. Sci. Instrum. 44, 1646 (1973).
[33]H. G. Alles, Ph.D. Thesis, University of Oregon, 1972 (available on microfilms, Ann Arbor, Mich., Dissertation No. 73-13, 721).
[34]R. A. Phillips and A. V. Gold, Phys. Rev. 128, 932 (1969).
[35]P. T. Coleridge and I. M. Templeton, J. Phys. F 2, 643 (1972).
[36]J. E. Graebner *et al., Magnetism and Magnetic Materials—1974,* edited by C. D. Graham, Jr., *et al.* (American Institute of Physics, 1975) p. 445.
[37]P. T. Coleridge and I. M. Templeton, Phys. Lett. 27, 344 (1968).
[38]In pure Rh, the LK limit $(2\theta-\theta_2)_{LK}=-45°$ on both $\alpha(111)$ and $\beta(100)$ orbits since $\cos(2\pi S)<1$, and the extremal areas for both orbits are maximum cross sections.
[39]T. A. Kitchens, W. A. Steyert, and R. D. Taylor, Phys. Rev. A 138, 467 (1965).
[40]N. Rivier and V. Zlatic, J. Phys. F 2, L87 (1972).
[41]N. Rivier and V. Zlatic, J. Phys. F 2, L99 (1972).
[42]H. Nagasawa, J. Phys. Soc. Jpn. 25, 691 (1968).